PCCP

Physical Chemistry Chemical Physics

www.rsc.org/pccp

Volume 12 | Number 16 | 28 April 2010 | Pages 3925–4256

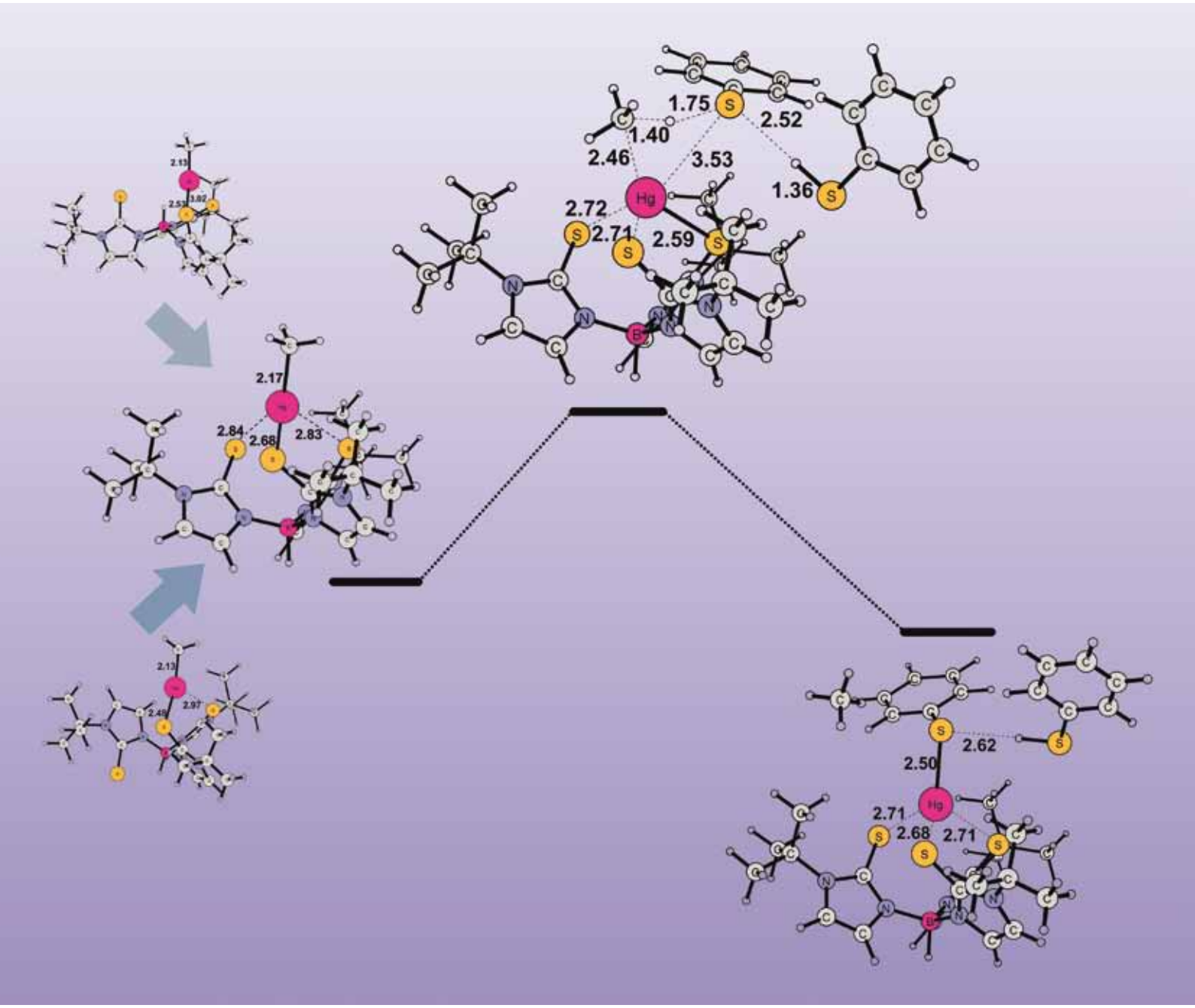

ISSN 1463-9076

COVER ARTICLE
Chen *et al.*
DFT studies of the degradation mechanism of methyl mercury activated by a sulfur-rich ligand

ARTICLE
Barone *et al.*
Parameterzation and validation of an accurate force-field for the simulation of alkylamine functionalized silicon (111) surfaces

1463-9076(2010)12:16;1-0

DFT studies of the degradation mechanism of methyl mercury activated by a sulfur-rich ligand†

Xichen Li,[a] Rong-Zhen Liao,[a] Wenchang Zhou[b] and Guangju Chen*[a]

Received 8th September 2009, Accepted 24th December 2009
First published as an Advance Article on the web 28th January 2010
DOI: 10.1039/b918402c

We describe theoretical insights into the mechanism of Hg–C bond protonolysis in methyl mercury coordinated by the tris(2-mercapto-1-*tert*-butylimidazolyl)hydroborato ligand, the structural and functional analogue of the organomercurial lyase MerB. Different cleavage pathways including both frontside and backside attack transition states were systematically studied by the hybrid density functional method B3LYP. Dependence of Hg–C bond activation on the primary sulfur coordination number of mercury was elaborated, and conceptual DFT indexes were suggested to be more appropriate than gross charge of atom sites in interpreting the dependence. Furthermore, absence of configurational inversion in MerB-catalyzed reactions was accounted for by examinations of the backside protonolysis pathways in the present system. Lastly, a rationalization was provided about the choice between different characteristics of transition states including both four-center and six-center ones.

Introduction

The widely distributed mercury and its compounds are extremely harmful to living organisms.[1–8] The protonolysis of the alkyl carbon–mercury bond is notoriously inert under physiological conditions; however, the natural organomercurial lyase MerB accelerates the protolytic cleavage by 10^6–10^7 fold.[9–14] (Fig. 1(a)).

Mechanistic studies of the MerB lyase are consequently important to improve the detoxification efficiency and to develop new remediation technologies. However, the roles of the crucial cysteine residues (Fig. 1(b)) and the identity of the proton donor in the catalytic mechanism of MerB have been controversial (Fig. 2(a)). Specifically, site-directed mutagenesis[17] and NMR spectroscopy[18–20] investigations indicate that one of the two conserved cysteine residues should serve as the Brønsted acid and concomitantly become liganded to Hg^{2+}; nonetheless, the pioneering enzymology studies[13,21,22] and recent X-ray crystallography research[15] suggest that both cysteine residues should focus on activating the Hg–C bond while Asp-99 should act as the proton donor (Fig. 2(b)), which was further supported by the recently published study of the MerB mechanism.[23]

Model studies have assisted the understanding of catalysis mechanism of MerB significantly. Experimental work on the acidic cleavage of substituted naphthalene mercurial using dithiols as ligands suggests that a carboxylic acid could serve as the acid donor[25] and supports Fig. 2(a1). Observations of the degradation of tetrahedral organomercury phosphane and thioether complexes, respectively, have demonstrated that multiple primary coordinations, by phosphane[26] or sulfur,[24] could play an important role in alkyl carbon–mercury bond protonolysis. Although with rather small computational models, theoretical studies have also provided important insights. It has been shown that increase of negative charges at the reactive methyl carbon site,[27–29] which could result from successive coordination of thiolates to Hg,[30] would facilitate protonolysis of the Hg–C bond. In addition, a frontside six-center transition state (TS) involving OH-containing residues, which could allow the formation of a second Hg–S bond and therefore would be energetically advantageous, has been proposed for the MerB-catalyzed protonolysis[24,31] (Fig. 2(a3)).

The systematic work targeting the tris(2-mercapto-1-*tert*-butylimidazolyl)hydroborato ([Tm$^{t\text{-Bu}}$]) and 1-*tert*-butylimidazole-2-thione ([Hmim$^{t\text{-Bu}}$]) ligand systems has been regarded as a breakthrough in searching for functional models of MerB.[31–34] Although the model system of the [Tm$^{t\text{-Bu}}$]HgR compounds might not fully exhibit the steric constraints of the MerB enzyme, their ability to react with PhSH rapidly to yield [Tm$^{t\text{-Bu}}$]HgSPh and RH at room temperature have demonstrated the facile cleavage of a carbon–mercury bond in a sulfur-rich coordination environment resembling closely the active site of MerB. The capability of [Tm$^{t\text{-Bu}}$] ligand to switch to higher-coordinate isomers, supported by ^{1}H NMR spectroscopic studies and two-dimensional exchange spectroscopy experiments, has been proposed to account for the exceptional reactivity (Fig. 3). However, the detailed protonolysis mechanism and the specific roles that the proposed configurational isomers play are not clear and need further investigations.

[a] *College of Chemistry, Beijing Normal University, 100875, Beijing, China. E-mail: gjchen@bnu.edu.cn; Fax: +86-010-58807971; Tel: +86-010-58807969*
[b] *Department of Biology, University of Konstanz, Universität Strasse 10, M647, D-78457 Konstanz, Germany*

† Electronic supplementary information (ESI) available: Full structures of frontside attack pathways featuring four-center, six-center and HB-assisted four-center TS for the [Tm$^{t\text{-Bu}}$] system, respectively. Full structures of backside attack pathways involving one and two PhSH molecules for the [Tm$^{t\text{-Bu}}$] system, respectively. Full structures of the frontside attack pathway featuring six-center TS for the [Hmim$^{t\text{-Bu}}$]$_{n=1}$ system. See DOI: 10.1039/b918402c

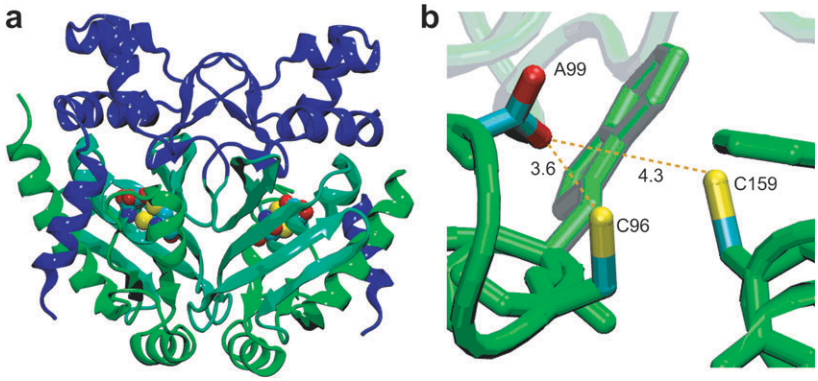

Fig. 1 The organomercurial lyase MerB. (a) Crystal structure of MerB[15] visualized by the VMD software.[16] For clarification, the color of the protein varies from blue to green starting from the N-terminus. Key residues Cys-96, Asp-99 and Cys-159 are highlighted. (b) Stereoview of the active site of the free MerB[15] visualized by the VMD software. The side chains of Cys-96, Asp-99 and Cys-159 are highlighted, together with the distances between the aspartic and cysteine residues (Å).

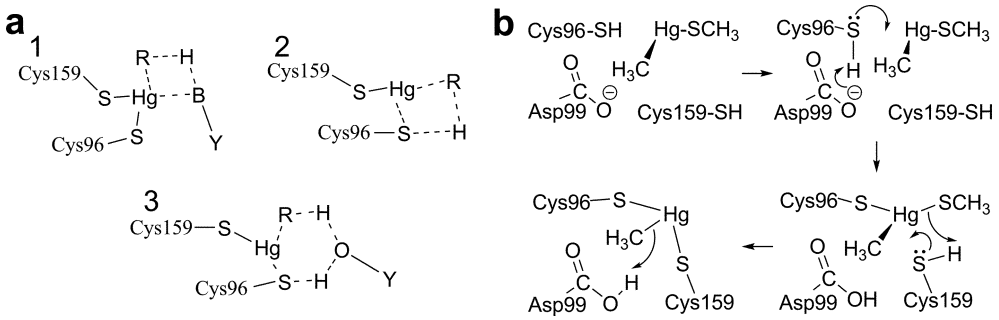

Fig. 2 (a) Controversial hypotheses of the protonolysis transition state, highlighting roles of conserved active-site cysteine residues. (1) Both conserved cysteines chelate Hg^{2+} to activate the Hg–C bond, and a third residue is responsible for the protic attack;[13,15,21–23] (2) The conserved Cys-159 serves as the primary ligand for RHg^{+}, and the other conserved cysteine, Cys-96 as proposed, protonates C and concomitantly forms another Hg–S bond.[17–20] (3) Similar to (2), but a hypothetically proposed OH-containing residue facilitates S–H deprotonation and concomitant protonation of the methyl carbon in the rate-determining transition state.[24] (b) Mechanism of MerB-catalyzed protonolysis of organomercurials proposed in the recent X-ray crystallography research.[15]

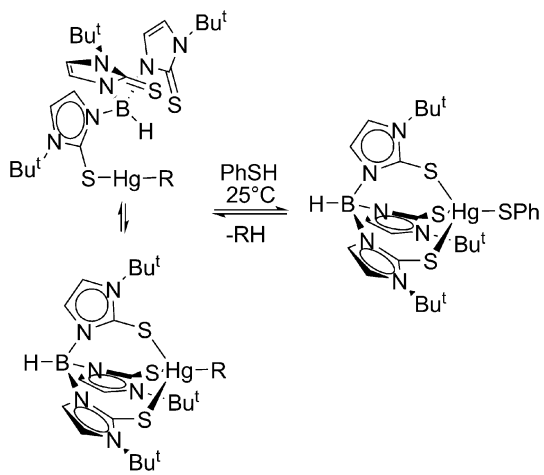

Fig. 3 The protonolysis reaction described in Melnick and Parkin's work.[32] The ability to switch to higher-coordinate isomers was proposed to account for the exceptional reactivity of the [Tm$^{t\text{-Bu}}$]HgR complex.

In this context, we focused on possible transition states and intermediates in the protonolysis of all the proposed κ^1, κ^2, and κ^3 coordination modes of [Tm$^{t\text{-Bu}}$]HgMe complexes ([$\kappa^1/\kappa^2/\kappa^3$-Tm$^{t\text{-Bu}}$]HgMe for short) to further the knowledge of the dependence of Hg–C bond activation towards effective protonolysis on mercury's primary sulfur coordination number. Because [Tm$^{t\text{-Bu}}$] has been regarded as the breakthrough structural and functional analogue of MerB, both the frontside and backside pathways have been examined to understand the absence of configurational inversion in MerB-catalyzed protonolysis (Fig. 4). Moreover, we have been examined two ways to assist the frontside four-center TS, namely six-center TS and hydrogen bond (HB)-assisted four-center TS, to evaluate the role of the proposed six-center TS in MerB-catalyzed protonolysis of organomercurials (Fig. 4).

Model and methods

Computation model

The initial geometrical parameters of the methyl mercury coordinated by [κ^1-Tm$^{t\text{-Bu}}$] ligand is extracted from CCDC #648328,[32] and shown in Fig. 5(a) with critical bond lengths. The κ^2 and κ^3 coordination modes were built up by manually

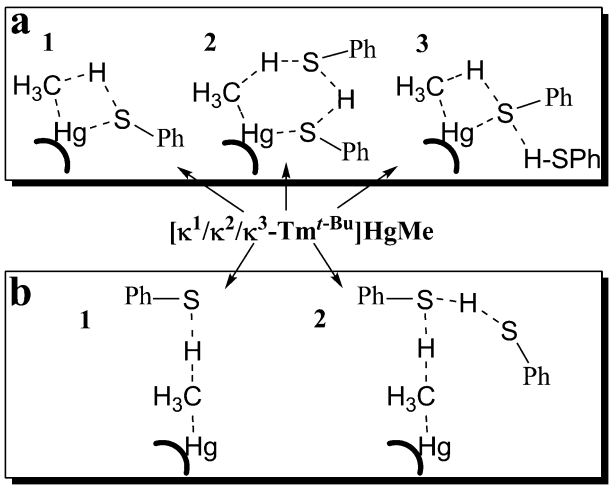

Fig. 4 Protonolysis transition states of [$\kappa^1/\kappa^2/\kappa^3$-Tm$^{t\text{-Bu}}$]HgMe studied in present study. The bold curve stands for the [$\kappa^1/\kappa^2/\kappa^3$-Tm$^{t\text{-Bu}}$] ligand. Panel (a) represents the frontside attack pathways: (a1) frontside four-center TS; (a2) frontside six-center TS; (a3) frontside HB-assisted four-center TS. Panel (b) represents the backside attack pathways: (b1) backside TS involving one PhSH; (b2) backside TS involving two PhSH. See text for further explanation.

adjusting the H–B–N–C dihedral angle to examine the participation of these isomers in the protolytic cleavage of methyl mercury.

Computational details

All calculations presented herein were performed employing hybrid DFT with B3LYP exchange–correlation functional[35–39] as implemented in the Gaussian 03 program package.[40] For geometry optimizations, the triple-ζ plus both polarization and diffuse functions basis set 6-311 + G(d) was used for sulfur atoms; the double-ζ plus polarization basis set 6-31G(d,p)[41–43] was used for the other non-metal atoms. Based on optimized geometries, more accurate energies were obtained by performing single-point calculations with larger basis set 6-311++G(2d,2p) for all the non-metal atoms. Throughout the calculations the SDD pseudopotential and valence basis set[42] have been employed for the mercury ion, the performance of which has been demonstrated in the recent literature.[24,44] Solvent effects were considered by performing single-point calculations on the optimized structures using the CPCM model.[45–48] In this model, the solvent is represented by a constant dielectric medium surrounding a cavity containing the solute. The solvent was chosen to be benzene according to the literature. For the basis set, calculations were first done at the levels of both geometrical optimizations and accurate energy calculations. Because the results were similar, the optimization level of basis set was employed throughout the solvent effects computations. Frequency calculations were performed at the optimization level of basis set to confirm the nature of stationary points, and to obtain zero-point corrections and the Gibbs free energies (*i.e.*, the term of the sum of electronic and thermal free energies). All energies herein are reported in two sets: electronic energies corrected for basis set, solvent, and zero-point vibrational effects, and Gibbs free energies with basis set and solvent corrections. BSSE corrections have been carried out with the Counterpoise keyword provided by Gaussian 03 package. For computations of the conceptual DFT indices in this paper, the SCF method has been employed to obtain the ionization potential (IP) and electron affinity (EA) according to the equations $I = E_{N-1} - E_N$, $A = E_N - E_{N+1}$, where

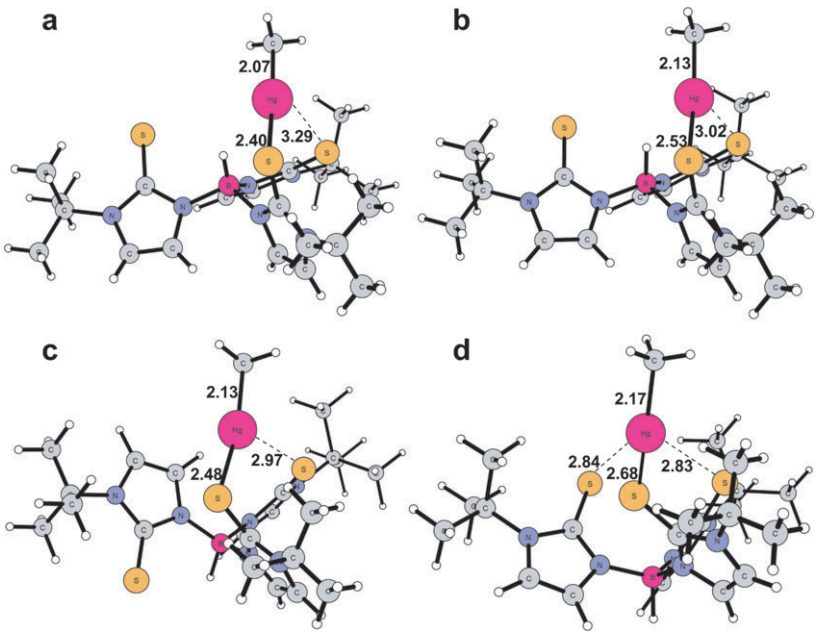

Fig. 5 Experimental and optimized structures: (a) [κ^1-Tm$^{t\text{-Bu}}$]HgMe from CCDC#648328; (b) optimized [κ^1-Tm$^{t\text{-Bu}}$]HgMe; (c) optimized [κ^2-Tm$^{t\text{-Bu}}$]HgMe; (d) optimized [κ^3-Tm$^{t\text{-Bu}}$]HgMe.

IP (I) and EA (A) are obtained from total electronic energy calculations on the $N-1$, N, $N+1$ electron systems, at the neutral molecule geometry.

Results

Geometrical conformation

The optimized structures of [$\kappa^1/\kappa^2/\kappa^3$-Tm$^{t\text{-Bu}}$]HgMe complexes as well as the experimental structure of [κ^1-Tm$^{t\text{-Bu}}$]HgMe extracted from CCDC #648328 are shown in Fig. 5. The κ^1 structure reproduces the experimental parameters. The difference of its primary Hg–S bond length 2.53 Å with the experimental value 2.40 Å is ascribed to the loss of periodicity in the computation model. The optimized κ^2 structure reflects the preference of [Tm$^{t\text{-Bu}}$]HgMe for κ^1 coordination mode.[32] Specifically, the two manually built primary Hg–S bonds change to 2.48 and 2.97 Å, respectively. For κ^3 structure, its Hg–S bonds are optimized to be 2.68, 2.83 and 2.84 Å, respectively. The elongation is consistent with the strong correlation between the Hg–S bond length and the sulfur coordination number of mercury.[49,50] Moreover, the bond length values show the system's preference for κ^1 coordination mode again.

Because it has been shown that B3PW91 and PBE1PBE yield geometries which are closer to MP2 and CCSD ones, especially where relatively weak interactions are involved, we also employed these functionals and results suggest that they provide basically the same structures with only slight differences.

Frontside four-center TS

Optimized structures of four-centre frontside attack TS and corresponding PRO for [$\kappa^1/\kappa^2/\kappa^3$-Tm$^{t\text{-Bu}}$]HgMe complexes are shown in Fig. 6. The energy profiles for [$\kappa^1/\kappa^2/\kappa^3$-Tm$^{t\text{-Bu}}$]HgMe complexes are shown in Fig. 7. The TS structures suggest that the electrophilic substitution happens from stretching of S–H bond of PhSH towards the activated carbon site. Specifically, from RE to TS structures, the average bond length of Hg–C bond of the complex and S–H bond of PhSH increase from 2.1 and 1.3 Å to 2.4 and 1.7 Å, respectively. The average bond length of complex–HPhSH reaches 1.4 Å in TS structures. Frequency calculations were carried out to confirm the nature of transition states to be the transfer of PhSH proton to methyl mercury carbon. In the PRO structures, the proton donor PhSH has its deprotonated sulfur coordinated to the mercury.

Electronic energy profiles show that the formation of RE complex for κ^1 mode is exothermic, while it is slightly endothermic for κ^2 and κ^3 modes (profile a, Fig. 7). In the subsequent protonolysis step, the κ^3 complex exhibits the lowest barrier, which should be attributed to the largest sulfur coordination number in κ^3 coordination mode. Free energy profiles suggest generally the same trend, except that the entropy effect has caused the formation energy of RE complex and the barrier to increase by 9.4 and 2.1 kcal mol^{-1} on average, respectively. Interestingly, in all the obtained TS structures, the mercury is coordinated by at least two sulfur ligands of the [Tm$^{t\text{-Bu}}$]. This phenomenon may reflect the requirement of mercury for a sulfur coordination number exceeding two to incur effective protonolysis of alkyl carbon–mercury bond.

Frontside six-center TS

Only for [κ^1/κ^2-Tm$^{t\text{-Bu}}$]HgMe complexes has the six-center TS been located. The optimized structures of TS and corresponding PRO are shown with critical bond lengths in Fig. 8. The energy profiles are provided in Fig. 7. For the sake of clarification, the PhSH which provides a proton to the methyl carbon in TS structures is referred to by PhSH1, and the PhSH providing proton to the PhSH1 sulfur is referred to by PhSH2. (The convention is used throughout the paper.) That is to say, PhSH1 functions in the same way as the proton donor PhSH in the frontside four-center TS described above, and PhSH2 should represent Y–OH in Strasdeit's notion.[24,31] Analysis of TS structures suggest that the initial proton attack happens directly from stretching of S–H bond of PhSH1; at the same time PhSH2 contributes its proton to PhSH1 and weakly coordinates to mercury. Specifically, the bond lengths of Hg–C, C–H_{PhSH1} and S_{PhSH1}–H_{PhSH1} change in a similar manner to those in the four-center situation. The average bond length of S_{PhSH2}–H_{PhSH2} only increases to 1.4 Å in the TS structures. The average bond length of S_{PhSH2}–Hg is 2.9 Å, suggesting its weak coordination interaction to mercury. Subsequent frequency calculations have confirmed that the transition states correspond to the transfer of PhSH1 proton to the methyl mercury carbon, with the minute displacement of the PhSH2 proton towards the PhSH1 sulfur. In the PRO structures, PhSH1 gets the proton from PhSH2, and the sulfur of PhSH2 coordinates to the mercury.

Similarly to the four-center situation, the clear dependence of protonolysis barrier on the sulfur coordination number of mercury has been demonstrated (profile b, Fig. 7). In addition, it has been confirmed again that the mercury ion is coordinated by at least two sulfur ligands in all the obtained TS structures. It should be noted that, concerning the free energy results, the average RE formation energy is larger than the four-center value by 13.0 kcal mol^{-1}, and the protonolysis barrier increases by 5.0 kcal mol^{-1} in average compared to the electronic energy value, which should be attributed to the additional entropy loss caused by introducing one more PhSH molecule according to the calculation results.

Frontside HB-assisted four-center TS

Attempts to find the frontside six-center TS for κ^3 complex have not succeeded as expected. Instead, a hydrogen bond (HB)-assisted four-center TS has been located, which has also been considered for κ^1 and κ^2 complexes. The optimized structures of TS and PRO are shown with critical bond lengths in Fig. 9. Energy profiles are shown in Fig. 7. Analysis of TS structures and subsequent frequency calculations suggest the transition state corresponds to the PhSH1 proton to methyl mercury carbon, with a stationary PhSH2 behaving as a pure

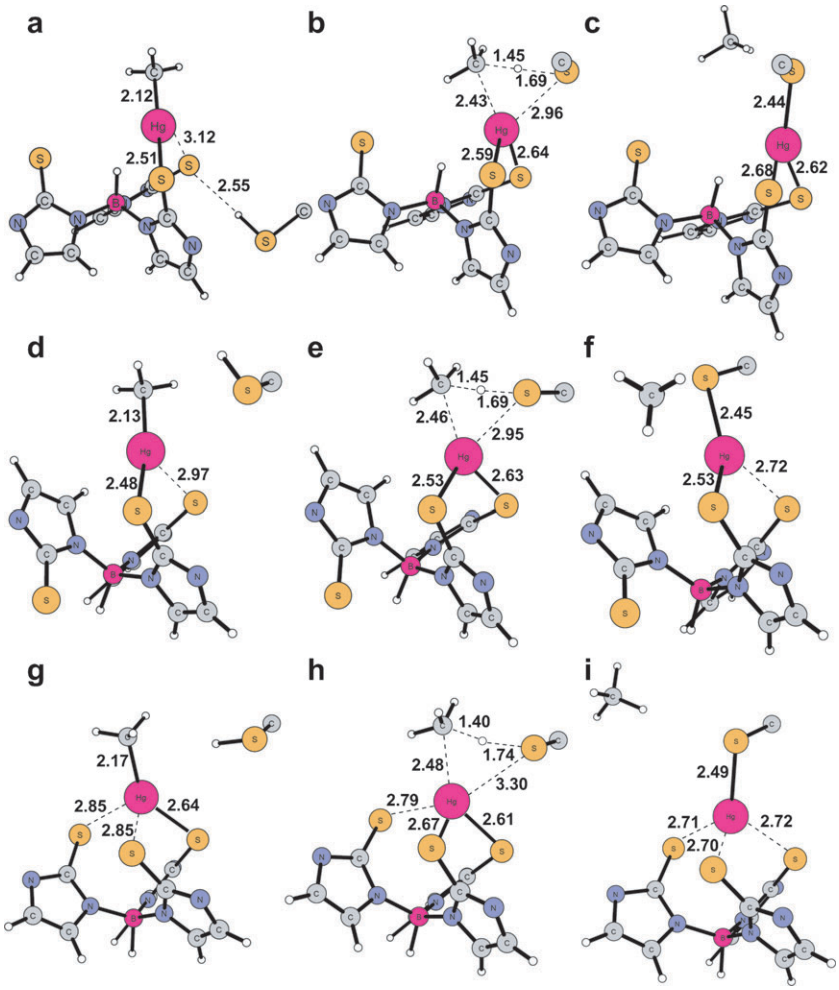

Fig. 6 Structures of the frontside attack pathway featuring four-center TS. (a), (d), (g): RE for [$\kappa^1/\kappa^2/\kappa^3$-Tm$^{t\text{-Bu}}$]HgMe complexes, respectively; (b), (e), (h): the corresponding TS; (c), (f), (i): the corresponding PRO. For clarity, the *tert*-butyl groups of the [Tm$^{t\text{-Bu}}$] ligand and the phenyl group of the thiophenol are omitted in the figures in the Results section. Figures with full molecules are provided in ESI.†

hydrogen bond donor to PhSH1. In the PRO, the PhSH1 sulfur coordinates to the mercury.

Clearly, the mercury being coordinated by at least two sulfur ligands in TS structures has been demonstrated again. Moreover, the electronic value of the protonolysis barrier for the κ^3 complex was calculated to be 25.9 kcal mol^{-1} relative to the free reactants (profile c, Fig. 7), which is the lowest one among all the studied frontside pathways. However, its free energy barrier increases considerably, which could be attributed to the entropy loss by introducing one more PhSH molecule.

Backside TS

Backside pathways, involving one or two PhSH molecules, of the protolytic cleavage of [$\kappa^1/\kappa^2/\kappa^3$-Tm$^{t\text{-Bu}}$]HgMe complexes have been investigated to understand the absence of this pattern in MerB-catalyzed protonolysis of organomercurials. The optimized structures of TS and PRO presented in Fig. 10 are only for the κ^3 complex for clarity, since the κ^3 coordination mode exhibited the lowest barrier compared to the other two modes. (The structures of backside attack pathway for [$\kappa^1/\kappa^2/\kappa^3$-Tm$^{t\text{-Bu}}$]HgMe complexes are provided in ESI.†) Barriers and reaction energies are listed in Table 1, where data of frontside pathways are also provided for comparison. TS structure analysis and frequency calculations have confirmed the validity of the protonolysis transition state. Unfortunately, as shown in Fig. 10, backside TS involving either one or two PhSH molecules failed to transform into the stable PRO and resulted in high-energy INT where the negative-charged sulfur of PhSH1 and positive charged mercury were screened apart. This may be ascribed to the long distance between the sulfur of PhSH2 and the mercury (5.6 Å in average).

Discussion

Dependence of the barrier of the protolytic cleavage of the alkyl carbon–mercury bond on the primary sulfur coordination number of mercury

In this work, three different coordination modes of the [Tm$^{t\text{-Bu}}$] ligand have been investigated to examine their

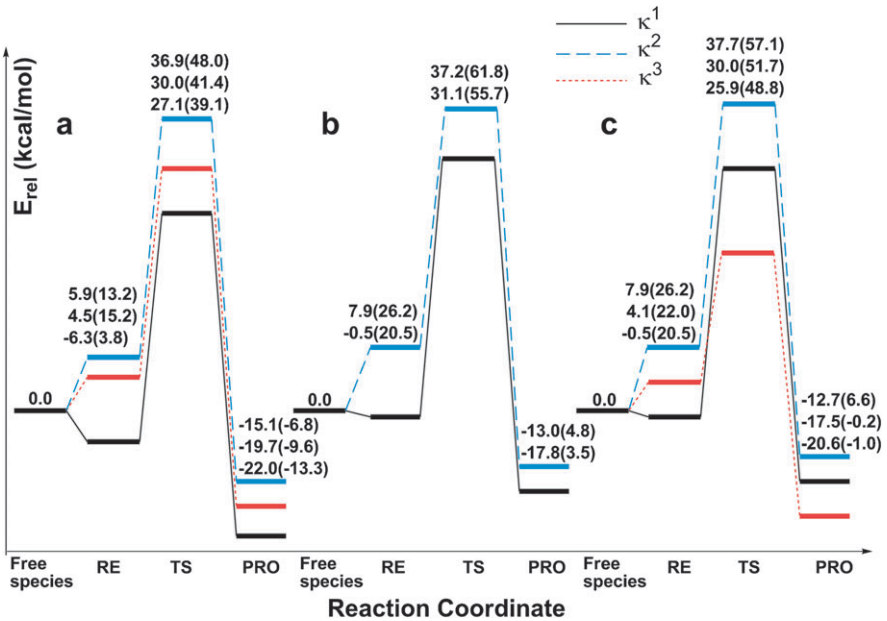

Fig. 7 Energy profiles for frontside attack pathways for [$\kappa^1/\kappa^2/\kappa^3$-Tm$^{t\text{-Bu}}$]HgMe complexes. Profiles a, b and c represent the frontside four-center, six-center and HB-assisted four-center pathways, respectively. The values outside the parentheses are electronic energies corrected for basis set, solvent, and zero-point effects, while the values inside the parentheses are Gibbs free energies with basis set and solvent corrections; the profiles are prepared based on the electronic energies corrected for basis set, solvent, and zero-point effects. It should be noted that, for clarity, because κ^1 and its isomers were proposed to be in rapid equilibrium,[32] we decided to leave out the small difference among the energies of free species of κ^1, κ^2 and κ^3 modes. That is to say, in preparing a certain profile, after calculating the formation energy of each RE complex with BSSE corrections individually, we aligned their zero values as depicted.

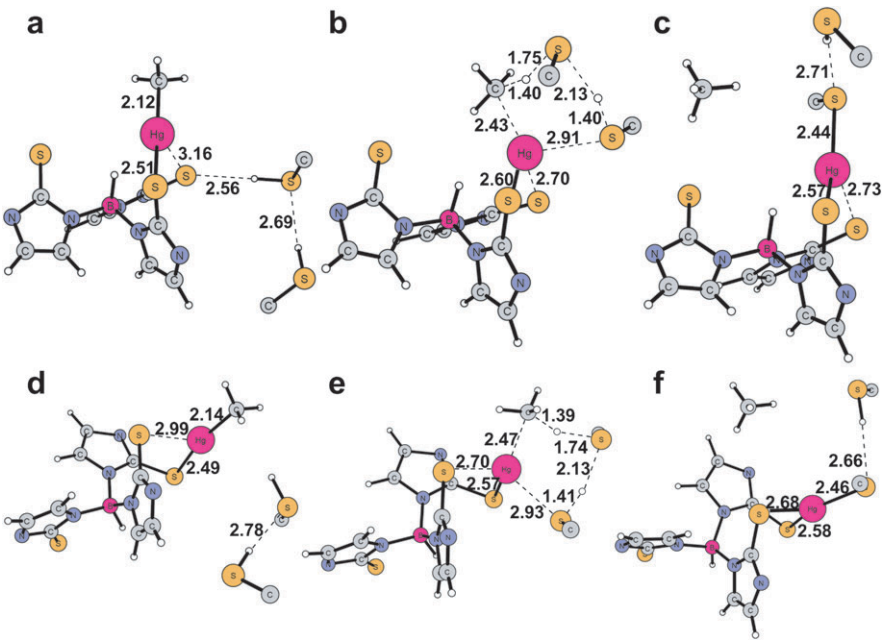

Fig. 8 Structures of the frontside attack pathway featuring six-center TS. (a), (d): RE for [κ^1/κ^2-Tm$^{t\text{-Bu}}$]HgMe complexes, respectively; (b), (e): the corresponding TS; (c), (f): the corresponding PRO.

impact on alkyl carbon–mercury bond protonolysis. Although PhSH might be a weaker proton donor than the aspartate residue of MerB, the understanding of the ligand's ability to allow the protonolysis at the room temperature should still contribute to the study of effective degradation of organomercurials. In all the studied pathways, the [κ^3-Tm$^{t\text{-Bu}}$]HgMe complex exhibited the lowest barriers in the protonolytic cleavage step compared

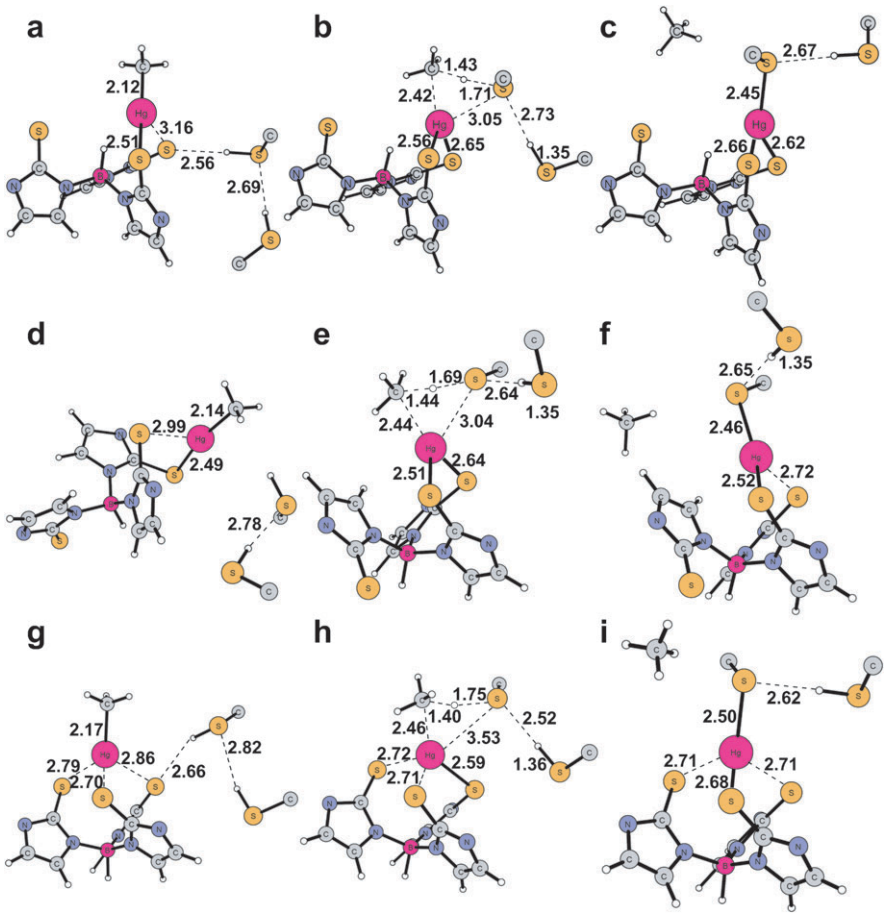

Fig. 9 Structures of the frontside attack pathway featuring HB-assisted four-center TS. (a), (d), (g): RE for [κ^1/κ^2/κ^3-Tm$^{t\text{-Bu}}$]HgMe complexes, respectively; (b), (e), (h): the corresponding TS; (c), (f), (i): the corresponding PRO.

to κ^1 and κ^2 counterparts, demonstrating clear dependence of protonolysis barrier on the primary sulfur coordination number of mercury. The reason why barriers for [κ^2-Tm$^{t\text{-Bu}}$]HgMe are much higher is that, as shown in Fig. 7, the formation of the corresponding reactant complexes are much more endothermic than the others. Furthermore, the mercury ion exclusively possesses at least two primary sulfur ligands in the obtained protonolysis transition states, indicating that a primary sulfur coordination number larger than two is necessary to incur effective protonolysis of the alkyl carbon–mercury bond. Therefore, our results suggest that both the conserved cysteine residues of the organomercurial lyase MerB, Cys-159 and Cys-96, should function mainly as primary ligands instead of the proton donor, which is consistent with the recent X-ray crystallography[15] and theoretical work.[23]

Because gross charge of atom sites has been used in related literatures to explain the reactivity difference,[28,30] NBO charges of the methyl carbon site in [Tm$^{t\text{-Bu}}$]HgMe isomers were calculated (Table 2). However, the obtained values were inconsistent with the barriers, probably because the sole usage of gross charges could not represent the electron density distribution of the reactive site. According to Klopman's notion,[51] the soft–soft reactions should be frontier controlled instead of charge controlled. To this end, the condensed-to-atom variants of the Fukui function,[52] the local softness,[53] and the local philicity[54] of [Tm$^{t\text{-Bu}}$]HgMe isomers have been calculated and demonstrated consistence with barriers (Table 2). Specifically, at the reactive methyl carbon site, much larger f_k^- was found in κ^3 complex than in κ^2 or κ^1 ones, and the κ^2 complex has similar f_k^- to the κ^1 complex. Because large value of f_k^- favors reactivity of the atom site towards electrophilic attack, the much lower protonolysis barrier of the κ^3 complex can be quite well rationalized. Moreover, the calculated indexes s_k^- and w_k^- suggest basically the same trend. Therefore, the dependence of the barrier of Hg–C bond protonolysis on the primary sulfur coordination number of should originate in the change of the frontier electron densities at the methyl carbon site when the mercury's primary sulfur coordination number changes.

Frontside attack *vs.* backside attack in the protonolysis TS

For the acidic cleavage of the alkyl carbon–mercury bond, the configurational retention pathway has been the preferred course in systems which have been investigated

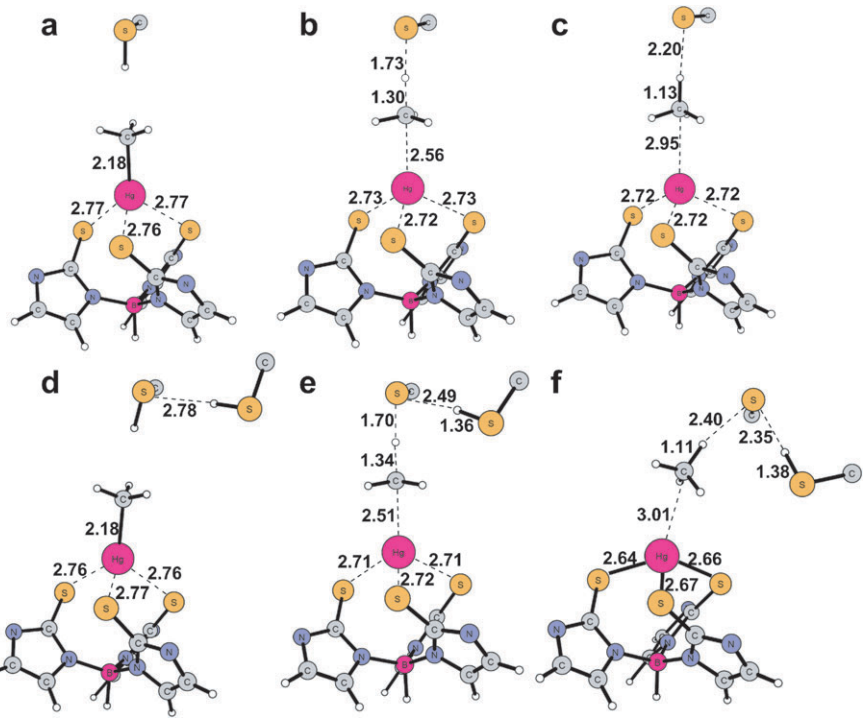

Fig. 10 Structures of the backside attack pathway for the κ^3 complex. (a), (b), (c): RE, TS and PRO involving one PhSH molecule; (d), (e), (f): RE, TS and PRO involving two PhSH molecules.

Table 1 Barriers and reaction energies of the studied pathways[a]

	Frontside			Backside	
Molecule	Four-center	Six-center	HB-assisted four-center	One PhSH	Two PhSH
[κ^1-Tm$^{t\text{-Bu}}$]HgMe	33.4 (35.3[b])	31.6 (35.2)	30.5 (31.2)	27.0 (28.6)	22.7 (25.7)
	−15.7[c] (−17.1)	−17.3 (−17.0)	−17.0 (−20.7)	29.0 (29.4)	24.0 (24.6)
[κ^2-Tm$^{t\text{-Bu}}$]HgMe	36.9 (48.0)	37.2 (61.8)	37.7 (57.1)	26.2 (26.7)	24.5 (22.6)
	−15.1 (−6.8)	−13.0 (4.8)	−12.7 (6.6)	27.3 (24.3)	24.3 (22.0)
[κ^3-Tm$^{t\text{-Bu}}$]HgMe	30.0 (41.4)		25.9 (48.8)	20.8 (21.0)	19.2 (20.0)
	−19.7 (−9.6)		−20.6 (−1.0)	19.7 (16.4)	14.5 (15.0)

[a] For clarity, in contrast to Fig. 7 where the sum of energies of free species are treated as zero, the barriers and reaction energies listed here are relative to the sum of energies of the free species energies if the energies of the corresponding REs are higher (for κ^2 and κ^3), and relative to energies of REs if they are lower (for κ^1). In this way, barriers of the protonolytic cleavage steps are more straightforward to analyze. [b] Values without parentheses are electronic energies corrected for basis set, solvent, and zero-point vibrational effects, while the values inside parentheses are Gibbs free energies with basis set and solvent corrections. [c] For each complex, the first line gives the barrier, and the second line shows the reaction energy.

Table 2 Local reactivity parameters of the reactive carbon site of [Tm$^{t\text{-Bu}}$] system

Molecule	q_N	f_k^-	s_k^-	w_k^-
κ^1	7.09617	0.01655	0.00299	0.03090
κ^2	7.12085	0.02653	0.00467	0.04690
κ^3	7.13616	0.09216	0.01647	0.19324

stereochemically.[13,21,22,55] In this work, efforts have been made to study possible transition states and intermediates in the backside attack protonolysis pathways to understand the absence of the backside style in related systems. Analysis of barriers suggests that the backside attack TS always requires less activation energy than the corresponding frontside attack TS (Table 1). (The word "corresponding" means the same coordination mode of [Tm$^{t\text{-Bu}}$] and the same amount of PhSH in comparison.) This is consistent with recent work by Ni and colleagues,[30] and has been attributed to the repulsion between positively charged species in frontside TS.[55] However, backside TS has lead to separation of positive and negative charges after the transition state of protolytic cleavage. Although efforts have been made in trying different reaction coordinates such as bending of Hg–C–S_{PhSH1} angle and so on, the expected proton exchange between PhSH molecules and subsequent transformation

Table 3 Wiberg bond indexes of selected atom pairs of the [Tm$^{t\text{-Bu}}$] system

Molecule		Hg–S_{48}	Hg–S_{49}	Hg–S_7	Hg–S_{PhSH1}	Hg–S_{PhSH2}
κ^1	Four-center	0.3261	0.2803		0.1752	
	HB-assisted four-center	0.3600	0.2790		0.1290	0.0023
	Six-center	0.3243	0.2427		0.0513	0.1534
κ^2	Four-center	0.3950	0.2807		0.1650	
	HB-assisted four-center	0.4148	0.2736		0.1288	0.0014
	Six-center	0.2553	0.3734		0.0548	0.1505
κ^3	Four-center	0.2541	0.3028	0.1946	0.0962	
	HB-assisted four-center	0.2249	0.3286	0.2286	0.0542	0.0022

into stable PRO failed to occur even if the ratio of PhSH to [Tm$^{t\text{-Bu}}$]HgMe reached two, which could be ascribed to the long distance between the sulfur of PhSH2 and the mercury ion (5.6 Å on average). Involvement of more PhSH molecules might facilitate the formation of stable PRO structures by shortening the distance, but should cause additional entropy loss in forming the reactant complex, and which factor is dominant would highly depends on the reaction system. Therefore, though the backside barrier tends to be lower than the frontside one, it is difficult for the backside TS to transform into stable PRO structures in the [Tm$^{t\text{-Bu}}$]HgMe system without introducing large entropy cost. This difficulty might account for the absence of the configurational inversion pathway in MerB and other related systems.

Does the frontside four-center TS need assistance?

Extensive enzymatic studies have demonstrated that enzymes reduce reaction barriers by stabilizing the transition states. Accordingly, it has been proposed that six-center TS involving an additional Y–OH residue would feature a second primary thiolate ligand to the mercury ion and thus lower the protonolysis barrier.[24,31] In this theoretical work on the [Tm$^{t\text{-Bu}}$] system, the functional analogue of MerB, both a frontside four-center TS involving one PhSH molecule, and a frontside six-center TS and HB-assisted four-center TS involving two interactive PhSH molecules, have been systematically studied to examine the assistance that the additional PhSH could bring.

(1) Electronic barriers for [κ^1/κ^3-Tm$^{t\text{-Bu}}$]HgMe were calculated as six-center TS $\approx$ HB-assisted four-center one $<$ four-center one, indicating that the additional PhSH molecule could assist the four-center TS. (As discussed in the above section, the much higher barriers for [κ^2-Tm$^{t\text{-Bu}}$]HgMe were attributed to the much more endothermic formation of the corresponding REs.)

(2) Attempts to locate the HB-enhancing four-center TS for the [Hmim$^{t\text{-Bu}}$]$_{n=1}$HgMe complex only results into the six-center TS (structures are provided in ESI†). This scenario corresponds to the model that Strasdeit *et al.* have employed in the quantum calculations,[24] where primary sulfur coordination numbers less than two in the reactant complex could not incur effective protonolysis of the mercury–carbon bond. Therefore, the six-center TS was calculated to be apparently advantageous because the PhSH provided an extra sulfur ligand.

(3) When the primary sulfur coordination number of mercury equals two in the TS structures of the κ^1 or κ^2 complex, the additional sulfur ligand that the PhSH2 would provide in the front six-center TS could merely bring weak coordination interaction (Table 3). Thus, the assistance brought by six-center TS was similar to that by HB-assisted four-center TS. Analysis of free energy results suggest almost the same trend, except that the barriers of protonolysis TS involving two PhSH molecules increase by 0.7 to 6.3 kcal mol^{-1} compared to the corresponding electronic energy values, because of the entropy loss in introducing the second PhSH. In related enzymatic reactions, however, the entropy effect could be reduced by the conformational adjustment of and the weak interactions within the enzyme.

(4) When the primary sulfur coordination number of mercury exceeds two (reaching three in the κ^3 complex in this work), the reactant complex gets another sulfur coordination interaction (Table 3) and thus would be easier for protonolysis than κ^1 or κ^2 complex. Furthermore, from the coordination chemistry point of view, the pseudo-tetrahedrally coordinated mercury would be already saturated and it could be hard for new-coming sulfur to get in. Therefore, the six-center TS might lose its value as allowing another sulfur ligand, and the HB-assisted four-center TS should be a better way to lower the reaction barrier, which could rationalize the absence of the six-center TS for [κ^3-Tm$^{t\text{-Bu}}$]HgMe complex reasonably.

Conclusions

In the present paper, we have systematically investigated the mechanism of the protolytic cleavage of Hg–C bond in methyl mercury activated by the [Tm$^{t\text{-Bu}}$] ligand, the breakthrough structural and functional analogue of the organomercurial lyase MerB. Protonolysis pathways involving all the proposed κ^1, κ^2 and κ^3 coordination modes of [Tm$^{t\text{-Bu}}$]HgMe have been carefully studied. Electronic barriers suggest that the frontside HB-assisted four-center TS of the κ^3 complex should be the most probable one in the original experiments. Our calculations have demonstrated the clear correlation between protonolysis barriers

and the primary sulfur coordination number of mercury. Conceptual DFT indexes were found more appropriate to interpret this correlation than gross charge of atom sites. Interestingly, it could be inferred from transition state structures that the primary sulfur coordination number should equal or exceed two to incur effective protonolysis. Moreover, careful examination of the backside pathways suggests that the difficulty to transform into stable product structures with minimum entropy loss should be responsible for the absence of configurational inversion in MerB-catalyzed degradations of organomercurials. Lastly, our results suggest that how the frontside four-center transition state can be assisted, and whether the six-center one is the right choice should be rationalized according to mercury's already-acquired coordination situation.

Acknowledgements

We appreciate Dr. Sven de Marothy (from Stockholm University) for providing the XYZ-Viewer to create the figures of the molecule models. We thank Prof. Per E M Siegbahn for his valuable advice. We thank Prof. Decai Fang for his instructive discussions. This work was funded by Science Foundation of National Science Foundation of China (Grant Nos. 20673011, 20503002 and 20631020), the Major State Basic Research Development Program (Grant No. G2004CB719900) and Canadian Institutes of Health Research where Prof. Z Jia provides kind help as a Canada Research Chair in Structural Biology.

References

1 J. O. Nriagu and J. M. Pacyna, *Nature*, 1988, **333**, 134–139.
2 J. O. Nriagu, *Nature*, 1989, **338**, 47–49.
3 T. W. Clarkson, *Annu. Rev. Public Health*, 1983, **4**, 375–380.
4 S. Silver and L. T. Phung, *Annu. Rev. Microbiol.*, 1996, **50**, 753–789.
5 F. M. M. Morel, A. M. L. Kraepiel and M. Amyot, *Annu. Rev. Ecol. Syst.*, 1998, **29**, 543–566.
6 *Recent Developments in Mercury Science*, ed. D. A. Atwood, Springer, Heidelberg, 2006.
7 W. F. Fitzgerald, C. H. Lamborg and C. R. Hammerschmidt, *Chem. Rev.*, 2007, **107**, 641–662.
8 J. Gailer, *Coord. Chem. Rev.*, 2007, **251**, 234–254.
9 A. M. Osborn, K. D. Bruce, P. Strike and D. A. Ritchie, *FEMS Microbiol. Rev.*, 1997, **19**, 239–262.
10 J. L. Hobman and N. L. Brown, *Met. Ions Biol. Syst.*, 1997, **34**, 527–568.
11 A. O. Summers, *Annu. Rev. Microbiol.*, 1986, **40**, 607–634.
12 T. Barkay, S. M. Miller and A. O. Summers, *FEMS Microbiol. Rev.*, 2003, **27**, 355–384.
13 M. J. Moore, M. D. Distefano, L. D. Zydowsky, R. T. Cummings and C. T. Walsh, *Acc. Chem. Res.*, 1990, **23**, 301–308.
14 T. W. Clarkson and L. Magos, *Crit. Rev. Toxicol.*, 2006, **36**, 609–662.
15 J. Lafrance-Vanasse, M. Lefebvre, P. D. Lello, J. Sygusch and J. G. Omichinski, *Biochemistry*, 2009, **284**, 938–944.
16 W. Humphrey, A. Dalke and K. Schulten, *J. Mol. Graphics*, 1996, **14**, 33–38.
17 K. E. Pitts and A. O. Summers, *Biochemistry*, 2002, **41**, 10287–10296.
18 P. Di Lello, G. C. Benison, H. Valafar, K. E. Pitts, A. O. Summers, P. Legault and J. G. Omichinski, *Biochemistry*, 2004, **43**, 8322.
19 G. C. Benison, P. D. Lello, J. E. Shokes, N. J. Cosper, R. A. Scott, P. Legault and J. G. Omichinski, *Biochemistry*, 2004, **43**, 8333–8345.
20 P. D. Lello, G. C. Benison, J. G. Omichinski and P. Legault, *J. Biomol. NMR*, 2004, **29**, 457–458.
21 T. P. Begley, A. E. Walts and C. T. Walsh, *Biochemistry*, 1986, **25**, 7186–7192.
22 T. P. Begley, A. E. Walts and C. T. Walsh, *Biochemistry*, 1986, **25**, 7192–7200.
23 J. M. Parks, H. Guo, C. Momany, L. Liang, S. M. Miller, A. O. Summers and J. C. Smith, *J. Am. Chem. Soc.*, 2009, **131**, 13278–13285.
24 M. Wilhelm, S. Deeken, E. Berssen, W. Saak, A. Lützen, R. Koch and H. Strasdeit, *Eur. J. Inorg. Chem.*, 2004, 2301–2312.
25 E. Gopinath and T. C. Bruice, *J. Am. Chem. Soc.*, 1987, **109**, 7903–7905.
26 P. Barbaro, F. Cecconi, C. A. Ghilardi, S. Midollini, A. Orlandini and A. Vacca, *Inorg. Chem.*, 1994, **33**, 6163–6170.
27 V. Barone, A. Bencini, F. Totti and M. G. Uytterhoeven, *J. Phys. Chem.*, 1995, **99**, 12743–12750.
28 V. Barone, A. Bencini, F. Totti and M. G. Uytterhoeven, *Organometallics*, 1996, **15**, 1465–1469.
29 V. Barone, A. Bencini, F. Totti and M. G. Uytterhoeven, *Int. J. Quantum Chem.*, 1997, **61**, 361–367.
30 B. Ni, J. R. Kramer, R. A. Bell and N. H. Werstiuk, *J. Phys. Chem. A*, 2006, **110**, 9451–9458.
31 H. Strasdeit, *Angew. Chem., Int. Ed.*, 2008, **47**, 828–830.
32 J. G. Melnick and G. Parkin, *Science*, 2007, **317**, 225–227.
33 S. M. Miller, *Nat. Chem. Biol.*, 2007, **3**, 537–538.
34 J. G. Omichinski, *Science*, 2007, **317**, 205–206.
35 C. Lee, W. Yang and R. G. Parr, *Phys. Rev. B: Condens. Matter*, 1988, **37**, 785–789.
36 A. D. Becke, *Phys. Rev. A: At., Mol., Opt. Phys.*, 1988, **38**, 3098–3100.
37 A. D. Becke, *J. Chem. Phys.*, 1992, **96**, 2155–2160.
38 A. D. Becke, *J. Chem. Phys.*, 1992, **97**, 9173–9177.
39 A. D. Becke, *J. Chem. Phys.*, 1993, **98**, 5648–5652.
40 M. J. Frisch, G. W. Trucks, H. B. Schlegel, G. E. Scuseria, M. A. Robb, J. R. Cheeseman, J. A. Montgomery, Jr., T. Vreven, K. N. Kudin, J. C. Burant, J. M. Millam, S. S. Iyengar, J. Tomasi, V. Barone, B. Mennucci, M. Cossi, G. Scalmani, N. Rega, G. A. Petersson, H. Nakatsuji, M. Hada, M. Ehara, K. Toyota, R. Fukuda, J. Hasegawa, M. Ishida, T. Nakajima, Y. Honda, O. Kitao, H. Nakai, M. Klene, X. Li, J. E. Knox, H. P. Hratchian, J. B. Cross, V. Bakken, C. Adamo, J. Jaramillo, R. Gomperts, R. E. Stratmann, O. Yazyev, A. J. Austin, R. Cammi, C. Pomelli, J. Ochterski, P. Y. Ayala, K. Morokuma, G. A. Voth, P. Salvador, J. J. Dannenberg, V. G. Zakrzewski, S. Dapprich, A. D. Daniels, M. C. Strain, O. Farkas, D. K. Malick, A. D. Rabuck, K. Raghavachari, J. B. Foresman, J. V. Ortiz, Q. Cui, A. G. Baboul, S. Clifford, J. Cioslowski, B. B. Stefanov, G. Liu, A. Liashenko, P. Piskorz, I. Komaromi, R. L. Martin, D. J. Fox, T. Keith, M. A. Al-Laham, C. Y. Peng, A. Nanayakkara, M. Challacombe, P. M. W. Gill, B. G. Johnson, W. Chen, M. W. Wong, C. Gonzalez and J. A. Pople, *GAUSSIAN 03 (Revision C.02)*, Gaussian, Inc., Wallingford, CT, 2004.
41 P. C. Hariharan and J. A. Pople, *Theor. Chim.Acta*, 1973, **28**, 213–222.
42 D. Andrae, U. Haeussermann, M. Dolg, H. Stoll and H. Preuss, *Theor. Chim. Acta*, 1990, **77**, 123–141.
43 T. Clark, J. Chandrasekhar and P. v. R. Schleyer, *J. Comput. Chem.*, 1983, **4**, 294–301.
44 H.-C. Tai and C. Lim, *J. Phys. Chem. A*, 2006, **110**, 452–462.
45 A. Klamt and G. Schueuermann, *J. Chem. Soc., Perkin Trans. 2*, 1993, 799–805.
46 J. Andzelm, C. Koelmel and A. Klamt, *J. Chem. Phys.*, 1995, **103**, 9312–9320.
47 V. Barone and M. Cossi, *J. Phys. Chem. A*, 1998, **102**, 1995–2001.
48 M. Cossi, N. Rega, G. Scalmani and V. Barone, *J. Comput. Chem.*, 2003, **24**, 669–681.
49 E. S. Gruff and S. A. Koch, *J. Am. Chem. Soc.*, 1990, **112**, 1245–1247.

50 J. G. Wright and H.-T. Tsang, *J. Am. Chem. Soc.*, 1990, **112**, 2434–2435.
51 *Chemical Reactivity and Reaction Paths*, ed. G. Klopman, Wiley, New York, 1974.
52 W. Yang and W. J. Mortier, *J. Am. Chem. Soc.*, 1986, **108**, 5708–5711.
53 W. Yang and R. G. Parr, *Proc. Natl. Acad. Sci. U. S. A.*, 1985, **82**, 6723–6726.
54 P. K. Chattaraj, B. Maiti and U. Sarkar, *J. Phys. Chem. A*, 2003, **107**, 4973–4975.
55 F. R. Jensen and B. Rickborn, *Electrophilic Substitution of Organomercurials*, McGraw-Hill, New York, 1968.